The Astrophysical Journal Supplement Series, 223:15 (10pp), 2016 March doi:10.3847/0067-0049/223/1/15

THE IBIS SOFT GAMMA-RAY SKY AFTER 1000 *INTEGRAL* ORBITS*

A. J. Bird[1], A. Bazzano[2], A. Malizia[3], M. Fiocchi[2], V. Sguera[3], L. Bassani[3], A. B. Hill[1], P. Ubertini[2], and C. Winkler[4]
[1] School of Physics and Astronomy, University of Southampton, SO17 1BJ, UK
[2] IAPS/INAF, Italy
[3] IASF/INAF, Bologna, Italy
[4] ESA-ESTEC, Research and Scientific Support Dept., Keplerlaan 1, 2201 AZ, Noordwijk, The Netherlands
Received 2015 July 31; accepted 2016 January 20; published 2016 March 30

ABSTRACT

Here we report an all-sky soft gamma-ray source catalog based on IBIS observations performed during the first 1000 orbits of *INTEGRAL*. The database for the construction of the source list consists of all good-quality data available, from the launch in 2002, up to the end of 2010. This corresponds to ∼110 Ms of scientific public observations, with a concentrated coverage on the Galactic Plane and extragalactic deep exposures. This new catalog includes 939 sources above a 4.5σ significance threshold detected in the 17–100 keV energy band, of which 120 sources represent previously undiscovered soft gamma-ray emitters. The source positions are determined, mean fluxes are provided in two main energy bands, and these are both reported together with the overall source exposure. Indicative levels of variability are provided, and outburst times and durations are given for transient sources. A comparison is made with previous IBIS catalogs and catalogs from other similar missions.

Key words: Galaxy: general – gamma rays: general – surveys

Supporting material: machine-readable table

1. INTRODUCTION

More than 11 years of observations in the energy range from 5 keV up to 10 MeV have been performed with the *INTEGRAL* observatory, which was selected as the M2 mission within ESA's Horizon 2000 program. The observing time of *INTEGRAL* is awarded competitively via a general program that is open to the community at large, and includes targets of opportunity, normal observations and key programs. The latter category consists of deep observations requiring a few Ms observing time, and may accommodate various requests from the observer community for amalgamated single targets or multiple targets within the selected sky fields. Typical observation times range between 100 ks and more than 2 weeks, and a number of the programs have provided regular monitoring of the Galaxy by returning to the same area of sky on multiple occasions.

Survey observations with *INTEGRAL* make full use of the large field of view of the IBIS coded mask telescope, one of the two main instruments on board the satellite. IBIS, with its large field of view (28 × 28°, 9 × 9° fully coded), excellent imaging, and spectral capability, is ideal for survey work (Ubertini et al. 2003). The imaging system provides a location accuracy of 0.′5–4′ depending on the source strength. For the large numbers of newly detected unidentified sources, these localizations are sufficiently good to enable searches for their soft X-ray counterparts. The results presented here are derived from ISGRI (Lebrun et al. 2003), the low energy array on IBIS, a pixelated CdTe detector operating in the energy band 17–1000 keV.

Since 2004, a sequence of IBIS survey catalogs (Bird et al. 2004, 2006, 2007, 2010) based on data from the ISGRI detector system have been published at regular intervals, making use of an ever-increasing data set as new observations become publicly available. The last edition of the IBIS survey (Bird et al. 2010), comprised of 723 sources, was released in 2010, and was based on *INTEGRAL* data collected between 2003 February and 2008 April. The overall content of this unbiased catalog comprised known active galactic nuclei (AGNs) (35%), X-ray binaries (31%), pulsars, and other sources (5%), while 29% of the sources were unknown or detected for the first time with *INTEGRAL*. A large number of observations at X-ray wavelengths with *Swift*, *XMM*, and *Chandra* followed, in order to obtain better position determinations and hence a more reliable optical identification. Other *INTEGRAL*-based catalogs have been produced, and focus on specific sky areas such as the Galactic Plane (Krivonos et al. 2010, 2012) or on specific source classes (Bassani et al. 2006; Lutovinov et al. 2007, 2013; Sazonov et al. 2007; Revnivtsev et al. 2008a, 2008b; Beckman et al. 2009; Scaringi et al. 2010a; Malizia et al. 2012). Another catalog produced in 2008 (Bouchet et al. 2008) was based on SPI (the other primary wide-field instrument on *INTEGRAL*) observations. Apart from just one variable source, all the objects listed in that publication were included in the fourth IBIS/ISGRI survey catalog (hereafter "cat4;" Bird et al. 2010).

The most recent *INTEGRAL* survey (Krivonos et al. 2012) is based on 9 years of averaged sky images and lists only those sources detected along the Galactic Plane ($|b| < 17.^\circ5$) in 3 energy bands (17–60, 17–35 and 35–80 keV); it includes 402 objects exceeding a 4.7σ detection threshold on the 9-year average map.

In all, the total number of *INTEGRAL*-discovered sources (i.e., those with an IGR designation) from the various catalogs up to the end of 2013 consists of ∼560 IGR detections, of which only 39% remain unidentified. In large part this unidentified fraction can be attributed to transient sources for which rapid follow-up was not available.

A noteworthy innovation is the SIX catalog (Bottacini et al. 2012), based on a new approach developed to survey the

* Based on observations with *INTEGRAL*, an ESA project with instruments and a science data center funded by ESA member states (especially the PI countries: Denmark, France, Germany, Italy, Switzerland, Spain), Czech Republic and Poland, and with the participation of Russia and the USA.

sky at hard X-ray energies (18–55 keV energy band) by combining the observations of *Swift*/BAT and *INTEGRAL*/IBIS to enhance the exposure time and reduce systematic uncertainties. This survey may be considered a survey from a virtual new hard X-ray mission, and should provide higher sensitivity than individual instrument surveys. The method has been applied to 6200 deg^2 of extragalactic sky (~20% of the entire extragalactic sky) and lists 113 sources, mostly of extragalactic nature: 91 AGNs, 2 clusters of galaxies, 3 Galactic sources, 3 previously detected X-ray sources, and 14 unidentified sources. Suppression of systematics is a key feature of this method, and no false detections due to statistical or systematic fluctuations are expected by the authors.

Here we present an update to the fourth IBIS/ISGRI catalog with data collected up to *INTEGRAL* orbit 1000, i.e., up to the end of 2010, that now comprise over 900 sources. For this updated database, we again made use of the "bursticity" tool to improve the detection of sources showing high variability and provide enhanced weak transient source detection. In particular, we use improved algorithms to provide a critical re-analysis of the methods used in Bird et al. (2010) and give additional quality flagging in order to reduce the expected levels of false detections in this new work. Details on the analysis and production of this new catalog (hereafter "this work" or "cat1000") are in Sections 2 and 3, and a comparison with the more recent similar catalogs is provided in Section 5.

2. DATA ANALYSIS AND CATALOG CONSTRUCTION

2.1. Input Data set

For this work, all publicly available *INTEGRAL* data obtained up to the end of 2010 have been processed. This may be compared to cat4, which used public data up to 2007 April (plus public and core program data up to 2008 April). During each satellite orbit (revolution; approximately three days) *INTEGRAL* operates by dividing each observation into a sequence of short pointings (science windows or scw) with a typical duration of 2 ks. Our data set extends from revolution 12 onward, and includes the performance verification, calibration, original core program (including Galactic Center deep exposure and Galactic Plane scans), and all pointed observations selected in the various observer AO phases up to revolution 1000 (2010 December). All data from revolution 12 onward were processed, unless flagged as bad time intervals (flagging is provided by the *INTEGRAL* Science Data Center, ISDC), for a total of ~73,000 scws (see 39,548 for cat4). The input catalog used was the *INTEGRAL* reference catalog v31, which includes all sources of the fourth IBIS/ISGRI catalog, further updated for any new *INTEGRAL* detected sources published via papers and ATELs since 2010. A final cleaning catalog containing all previously declared *INTEGRAL* detected sources was created and used as the input catalog for all pipeline processing.

The total exposure in the data set (the sum of exposures of all initially selected scw) is 124 Ms (see 70 Ms in cat4), and the resulting all-sky exposure distribution is shown in Figure 1 (upper panel).

As a result of the core program and key programs that operated from 2006, the Galactic Bulge is well-covered, with ~12 Ms, and the entire Galactic Plane has a coverage of at least 300 ks, rising dramatically in areas where specific sources have been targeted. The Galactic anti-center region has been less

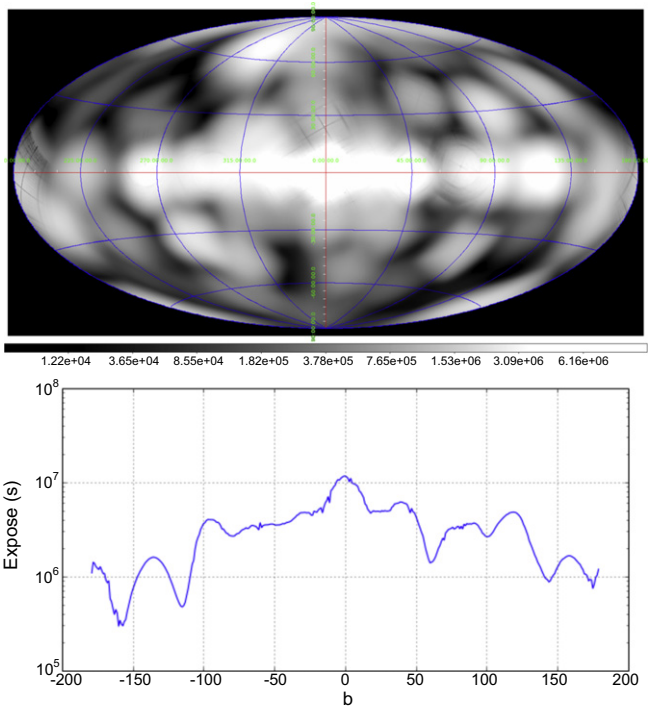

Figure 1. (Upper panel) Overall exposure map for 18–60 keV processing; the features of residual filtering (Section 2.2.1) can be seen around the positions of the brightest sources. (Lower panel) The exposure along the Galactic Plane resulting from all exposures, but dominated by the Galactic Bulge and Galactic Plane scan programs.

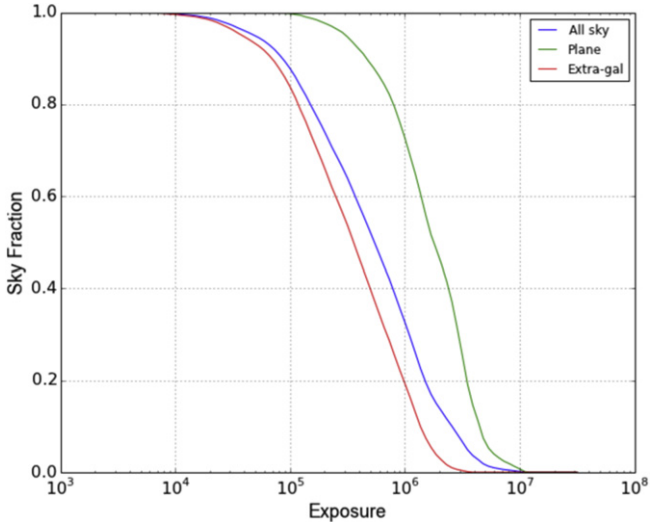

Figure 2. Fraction of the sky covered as a function of exposure time.

well-covered due to mission planning constraints, as this region is competing with the Galactic Center for observing time. The exposure profile along the Galactic Plane is shown in Figure 1 (lower panel).

The fraction of sky exposed to a certain level is shown in Figure 2, which emphasizes the different exposure patterns in the Galactic Plane ($|b| < 15°$) and the extragalactic sky ($|b| > 15°$). In the Galactic Plane, 75% of the sky is covered to better than 1 Ms, while only 20% of the extragalactic sky is covered to the same level. Overall, around one-third of the sky

is covered to a 1 Ms level, and 90% of the sky is covered to 100 ks.

2.2. Data Processing and Pipeline Processing

The data processing was performed with the Standard OSA 9.0 software to produce sky images of individual scws in five different energy bands (17–30, 30–60, 18–60, 20–40 and 20–100 keV). For mosaic construction, source searching, candidate list production, and final source selection we have been largely following the fourth IBIS catalog procedure as described in Bird et al. (2010). In the following sections, we only report the main changes with respect to the earlier methodology.

2.2.1. Mosaic Construction

Each scw image was tagged with its rms (after removal of sources) to act as an indicator of overall image quality. The primary aim of this step is to remove data taken during periods of enhanced background during solar activity or soon after perigee passage. Filtering was applied based on the rms value of the image background, such that the rms should not exceed a limit of 2σ above the mean image rms for the whole data set. This function somewhat overlaps with the BTI flagging provided by the ISDC, but we still removed around 5400 of the science windows that exceed this rms limit, for a loss of 11 Ms or 8% to the total exposure. We note that there is a clearly increasing trend in the image rms throughout the mission, especially in the energy bands extending below 20 keV. In future analyses, an adaptive time-varying rms filter may be required if this trend continues, but for now we used a constant threshold, and accepted a slightly higher rejection fraction in the later parts of the mission.

Although they are still processed, data taken in staring mode are not used in the construction of the final sky mosaic images, as they contribute a far higher level of systematic noise than the standard dithered observations (although this effect is less pronounced from OSA 9 onwards). Some 1290 science windows in the input data set were flagged as consisting of staring data, representing a further exposure loss of 3.2 Ms (2.5%) in map construction.

After the removal of high-rms and staring data, approximately 67,000 scws remained in the data set, with a total exposure of ~110 Ms. The selected science windows were then combined using a proprietary image mosaic tool that statistically averages the images from multiple input maps. This process has been optimized to allow for the creation of all-sky maps based on large numbers of input science windows. Mosaics were constructed for 5 energy bands (see Section 2.2) with 2′.4 pixel resolution, significantly oversampling the intrinsic system point-spread function (PSF). Mosaics were made in four projections: centered on the Galactic Center, on the Galactic anti-center, north Galactic polar, and south Galactic polar. These multiple projections are intended to present the automatic source detection algorithms with source PSFs with the minimum possible distortion.

Previous catalogs have employed various timescales on which mosaics were constructed in an attempt to optimize the detection of new sources with a variety of duty cycles. We have simplified our approach, and initially constructed mosaics on only revolution and whole-archive timescales. Revolution maps are optimized to detect sources active on timescales of the order of a day and persistent sources can best be detected in an all-archive accumulation of all available high-quality data.

2.2.2. Candidate List Construction

Maps were searched with two different algorithms, the standard SExtractor tool (Bertin & Arnouts 1996), and an algorithm designed specifically to compensate for the varying levels of systematic background found in *INTEGRAL*/IBIS mosaics. In total, 60 all-sky maps (and variants) and over 19,000 revolution maps were constructed and searched. An initial candidate source list was created by iteratively merging the excess lists from each map into a base list that took the cleaning catalog as a starting point. In this way, merging commences with the best reference positions for each source, and the process also ensures that all previously declared sources are checked for their presence in the new data set. A merge radius of 8′ was used, and a new candidate was added to the base list if it exceeded a detection threshold of 4.5σ in an all-archive map, or 6σ in a revolution map, and could not be associated with an already listed source. The higher threshold for revolution maps is essential to remove false excesses caused by noise in these lower exposure maps. In addition to this higher threshold for revolution map excesses, a number of revolutions[5] were excluded from this process due to high noise levels associated with solar activity, these being 124–129 (inclusive), 217–218, 234, 252–254, 276–277, 315, 341–342, 349, 352–356, and 506–509. This process resulted in a list of 3759 excesses that was manually inspected to ensure that blended sources flagged in previous catalogs survived the merging process.

2.3. Final Source List Construction

Light curves were constructed for every candidate source in the five standard energy bands. A search for variable source emission was then performed on those light curves by using the "bursticity" method—i.e., identifying the time window within which the source significance was optimized. Time windows in the range 0.5 days up to the full duration of the light curve were tested. Once the optimum detection time window was determined, an additional map—the "burst map"—was constructed by mosaicking only those scw falling in the best time interval and using the energy band established by "bursticity." This method optimizes the detection of any known or suspected source that emits on any timescale longer than a science window. Following this procedure, an improved significance has been obtained for ~200 sources.

The final source list filtering was carried out manually. Experienced operators were presented with all the relevant data —as well as visual inspection of the maps themselves, derived parameters such as persistent significance in five energy bands, burst significance and timescales in five energy bands, local systematic levels, local image residual levels, and the total number of maps each source was detected in were quantified. A final acceptance of each putative source was made on the basis of this overall data. The overall flow of data through the analysis chain is shown in Figure 3, which also shows the selection/rejection criteria applied at each stage.

[5] Revolution dates can be found at http://www.cosmos.esa.int/web/integral/schedule-information

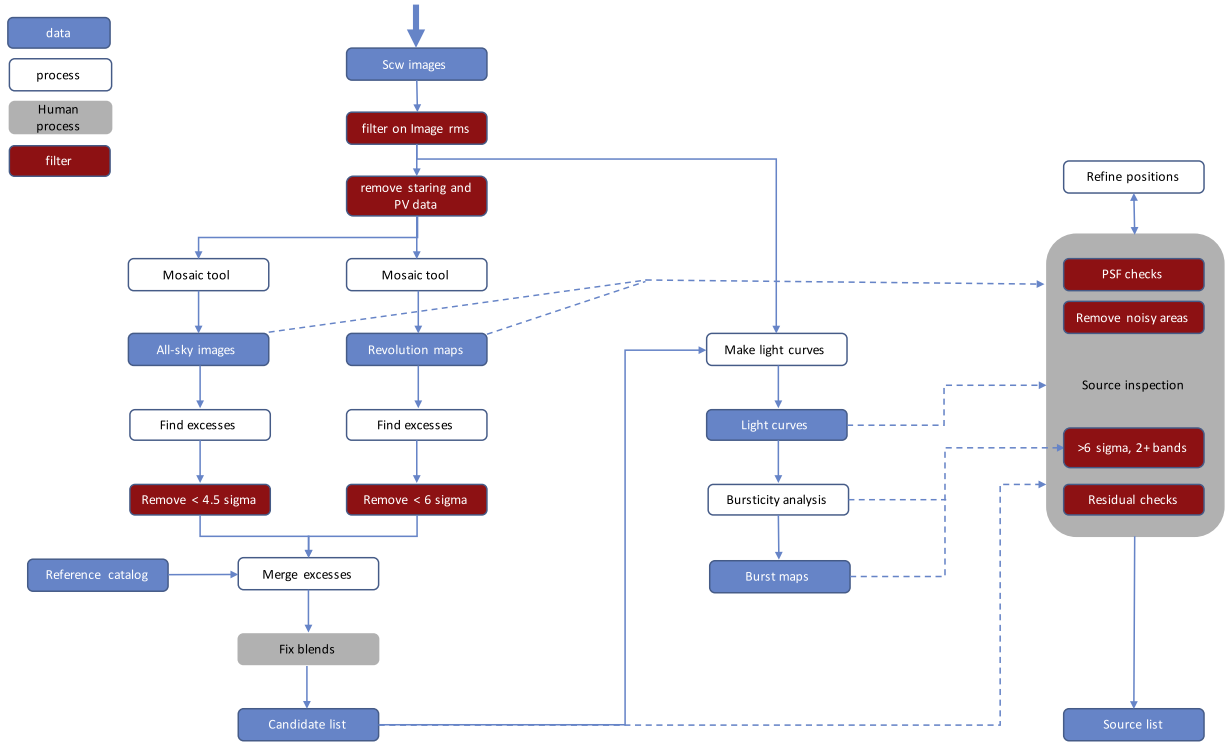

Figure 3. Data analysis and source selection flowchart, showing the filtering criteria applied at each stage.

2.4. False Positive Rates (FPRs)

The FPR (the fraction of "fake" sources in the catalog) is a key parameter, and depends strongly on the methods used to identify, examine and verify the excesses.

The FPR for persistent sources found in inspection of IBIS mosaic images has been well-established for previous catalogs (Bird et al. 2004, 2006, 2007, 2010; Krivonos et al. 2010) and can be quantified by inspecting a histogram of either the pixel significance values in the mosaics, or the significances of the detected excesses. We follow the method of cat4 and fit the pixel distribution (Figure 4) with a Gaussian noise component and a power-law component representing the sources. The point at which the noise population contributes ∼1% of the source population can therefore be estimated at between 4.5σ and 5σ, and these values have typically been used in prior catalog constructions. In this work, the threshold for 1% FPR is 4.8σ, the same as that quoted for cat4, though above the formal 4.5σ threshold; a total of 2.6% of the sources may be due to the noise component. We note, however, that in the significance range between 4.5σ and 4.8σ, the fraction of false sources may be as much as 25%, and we have indicated this in the table with a WARN flag.

The FPR arising from the bursticity method is much harder to quantify. Many trials are performed each time a light curve is tested, and the confidence levels for any "detection" must therefore be assessed carefully. An analytical approach to this is unlikely to yield a satisfactory result, as the ∼3000 light curves tested are of markedly different lengths and temporal structures (the data gaps come from the observing strategy of the telescope). Since both length and structure of the light curve affect the number of valid trials performed, they also affect the confidence limits, and we should formally assign limits on each light curve, but this is too cumbersome, and we adopt a simulation approach on the ensemble of light curves.

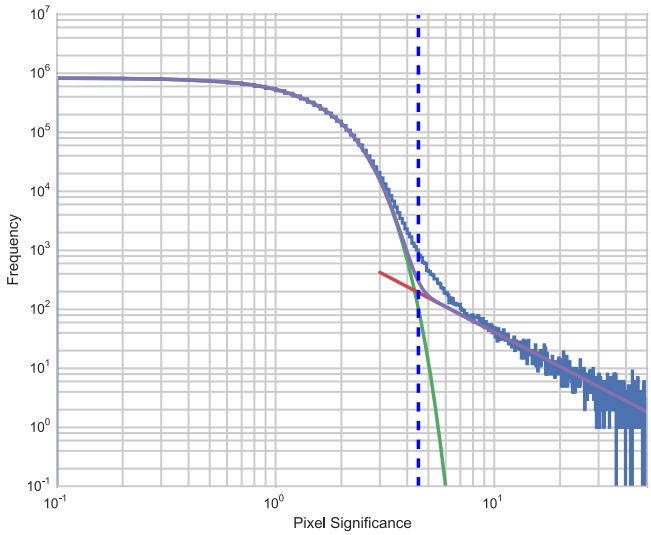

Figure 4. Pixel significance distribution for the 18–60 keV all-sky mosaic significance map. The distribution is modeled as a sum of noise (green) and source (red) contributions. The dashed vertical line is at 4.5σ.

We created new light curves by randomization of existing light curves that were selected to have no source signal. For a light curve containing N data points, N swaps of (time, flux/error) pairs were performed to randomize the light curve while retaining the original overall time structure. The advantage of this method is that a very large number of random light curves can be generated. However, the assumption in this method is that the noise in the light curve is purely statistical white-noise, as any correlated noise would be removed by the randomization.

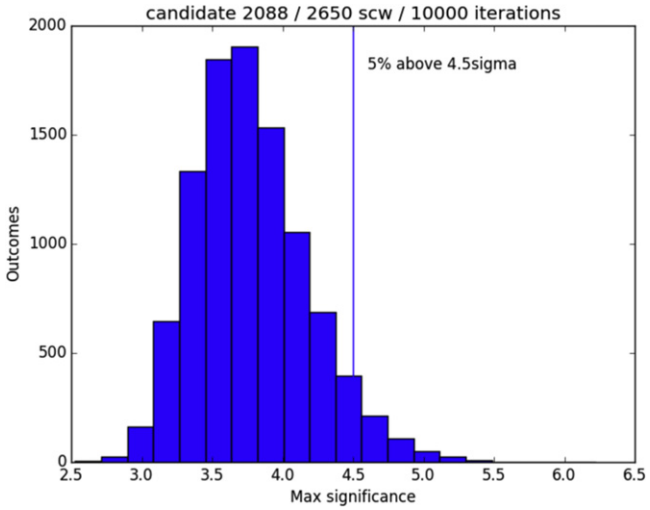

Figure 5. Maximum burst significances discovered in 10,000 randomly generated light curves containing 2650 science windows with a realistic time structure and noise distribution.

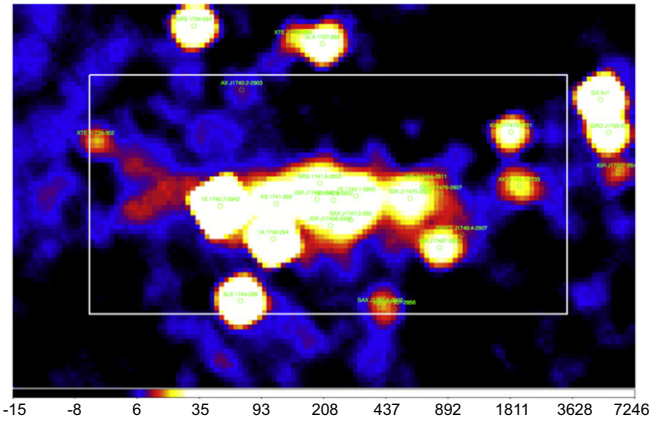

Figure 6. IBIS/ISGRI mosaic significance map of the Galactic Center region and resulting sources from the analysis. The white box represents the central $4^\circ \times 2^\circ$ region.

The distribution of burst significances detected in 10,000 randomized light curves derived from a medium length (2650 scw) light curve is shown in Figure 5. For this typical light curve length, 10% of the "bursticity" tests resulted in a detection above 4.5σ. Corresponding values for short (550 scw) and long (10,700 scw) light curves were 0.1% and 10%, respectively. In all these tests, less than 1% of iterations generated a detection above 6σ.

We performed a second set of simulations based on inversion of the ~3000 excess light curves. Each source flux light curve was subjected to a sigma-clipping algorithm to remove bright positive detections above the 5σ level, and then inverted about zero flux. In the assumption that the noise flux distribution from coded mask deconvolution is Gaussian distributed around a mean of zero, this results in light curves with the same noise and time structure as the original light curves. These light curves will retain any systematic noise and also will maintain any longer-term noise structures (red noise) present in the originals, but should effectively contain no signal flux. Analysis of these light curves should represent a worst case scenario in terms of the derived FPR when compared to the purely statistical, white-noise light curves made in the first approach. Using this approach, a "burst" of greater than 4.5σ is seen in 12.7% of the light curve analyses, and a "burst" of greater than 6σ is seen in 3.5% of the light curve analyses; this falls to 2% at the 7σ level.

Combining the results of these two simulation approaches, we can estimate that the mean false alarm rate above a 6σ threshold is between 1% (statistical best case) and 3.5% (systematic worst case) for a single light curve. Once we impose the additional requirement that the bursts are temporally aligned in more than one energy band, the statistical probability falls enormously due to the small burst duration, compared to the overall light curve length. In a purely statistical sense, even above 4.5σ the probability falls to <1%, as typical burst durations are <1% of the light curve duration. However, we must caution that some of the systematic effects occasionally seen (e.g., poor ghost source removal) will potentially generate noise simultaneously across all bands, so the final inspection processes are still vital to remove "ghosts" and areas of noise in maps. We pessimistically assume a final 1% FPR in the overall bursticity method when requiring simultaneous bursts in more than one band. Based on these simulations and our experience from cat4, we believe the false positive probability for sources detected on short timescales (<70 days) and at low significance is higher than the overall levels, and we have again indicated this in the table with a WARN flag. See Section 4 and Figure 7 for further information.

Overall, we estimate the FPR in this catalog is <25% for sources detected between 4.5σ and 4.8σ in persistent maps, <1% for sources detected above 4.8σ in persistent maps, and (pessimistically) 1% for sources detected via the bursticity method. Thus we anticipate ~30 false positives in a catalog of 939 sources, i.e., 3.5%, with a roughly equal number coming from each detection method.

2.5. Galactic Center Localizations

The central $4^\circ \times 2^\circ$ region of the Galaxy represents a challenging area for the *INTEGRAL*/IBIS map analysis (Figure 6). The presence of unresolved sources (and presumably many sources below the formal detection threshold creating a non-uniform background) means that the maps in this area are dominated by systematic effects and the usual statistical limits for source discovery do not apply. As a consequence, we have been extremely conservative in this region, and in fact all the sources listed are already present in the *INTEGRAL* Reference Catalog. Because of the complex and unresolved source distribution, the data quality for these sources may be lower than for isolated sources away from the Galactic Center. In the source list, we indicate this with a flag (GCFLAG) with the following two values. GCFLAG = 1 means that the source lies within the GC box, and is detected by our standard methods. Furthermore, the source is sufficiently resolved that we can estimate the flux and position from our maps; nevertheless we expect that the detection may be affected by nearby unresolved faint sources and the quantitative data should be treated with caution. GCFLAG = 2 means that there is clear evidence of emission from the source position in one or more of our maps, but it lies within an unresolved emission region. Therefore we cannot unambiguously attribute the emission to the source, and we therefore supply the reference catalog position only. The fluxes are almost certainly contaminated by emission from

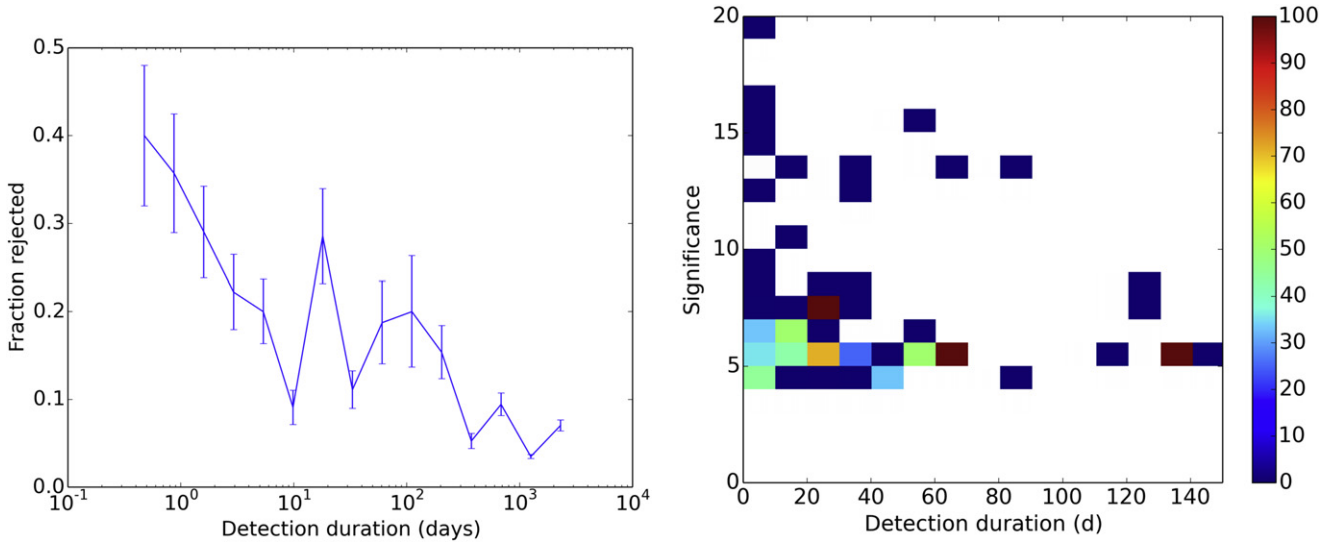

Figure 7. Analysis of the false positive rates for the transient detection performed in cat4. A cat4 source is rejected as potentially a false positive if it cannot be recovered by the improved and more stringent acceptance criteria used in this work. (Left panel) The fraction of sources rejected as a function of the source detection duration shows a clear trend toward more false positives for shorter outbursts; error bars indicate statistical uncertainties due to source numbers. (Right panel) Adding the source significance as a second parameter shows that short, low-significance outbursts contribute a very high fraction of the rejected sources.

nearby unresolved sources, or indeed resolved ones—in one case, two nearby sources (SAX J1750.8–2900 and IGR J17507–2856) are blended in stacked images of the region, but may be temporally identified because they outburst at different times, and the derived positions are unambiguously different. Nevertheless, cross-contamination of fluxes in this region is an ever-present problem. Using this approach, there are 23 sources falling within the Galactic Center zone, of which 11 have GCFLAG = 2.

We have cross-checked our results and sources in this area with the results from the bulge monitoring project[6] which provides a more regular monitoring and thus regularly detects transient sources; nevertheless, we have no real contradictions with their database. The differences that do exist, apart from occasional naming differences, are in fact due either to sources detected after revolution 1000 or to our detection acceptance threshold.

3. THE TABLE DATA

The name of the source is given following the convention to quote, wherever possible, the name declared at the time of the first X-ray detection. The names are given in bold for the ∼300 sources added to the catalog since cat4.

The astrometric coordinates of the source positions were extracted from the mosaics by the barycentering routines built into SExtractor 2.5. In almost all cases, the position for a source was extracted from the map yielding the highest source significance. In a few cases, primarily for blended sources, other maps were chosen in order to minimize the interference of other sources. Simultaneous fitting of multiple Gaussian PSFs was used in the most difficult cases—these sources are indicated as blended in the notes accompanying the table. The point source location error of IBIS is highly dependent upon the significance of the source detected (Gros et al. 2003; Scaringi et al. 2010b). We use the formulation of Gros et al. (2003), combined with the significance of the detection used to locate the source, in order to define an error on the source position. The source localization errors quoted are for the 90% confidence limit.

The mean fluxes quoted in the table as $F_{20–40}$ and $F_{40–100}$ are the time-averaged fluxes over the whole data set derived in two energy bands (20–40 and 40–100 keV). These are provided for compatibility with past catalogs and as a general reference value. However, as previously noted, their relevance as an average measure diminishes as the data set increases and the average time of activity for many of the sources is much shorter than the on-source exposure. For variable sources, we provide a variability indicator: a flag of Y indicates a bursticity >1.1 (i.e., a 10% increase in significance can be obtained by selecting a single contiguous subset of the data) and a slightly variable source. A flag of YY indicates a bursticity of >4 (i.e., a 400% increase in significance), indicating a strongly variable source. The significances quoted are the highest significance in any single map, since this gives the best indication of the robustness of source detection. However, it should be noted that the flux and significance values may derive from different energy bands and/or subsets of the data, and may initially appear contradictory. A brief commentary indicates the detection method for each source—here the term "persistent" means that the source detection is optimized in a mosaic of all data, but the detection may actually derive from a number of outbursts or flares, but no single outburst optimizes the detection. For sources detected during an outburst, the MJD and duration are indicated. Warning flags are appended to some sources to indicate their positions in the Galactic Center, or to warn of detections subject to higher FPRs due to lower significance or shorter duration (see Section 2.4).

The type of the source is encoded into up to four flags, which are explained in the table footnotes. We have followed the convention of (Liu et al. 2007) wherever possible. The exposure quoted is the total effective exposure on the source after all filtering of the data has been carried out.

[6] http://integral.esac.esa.int/BULGE/

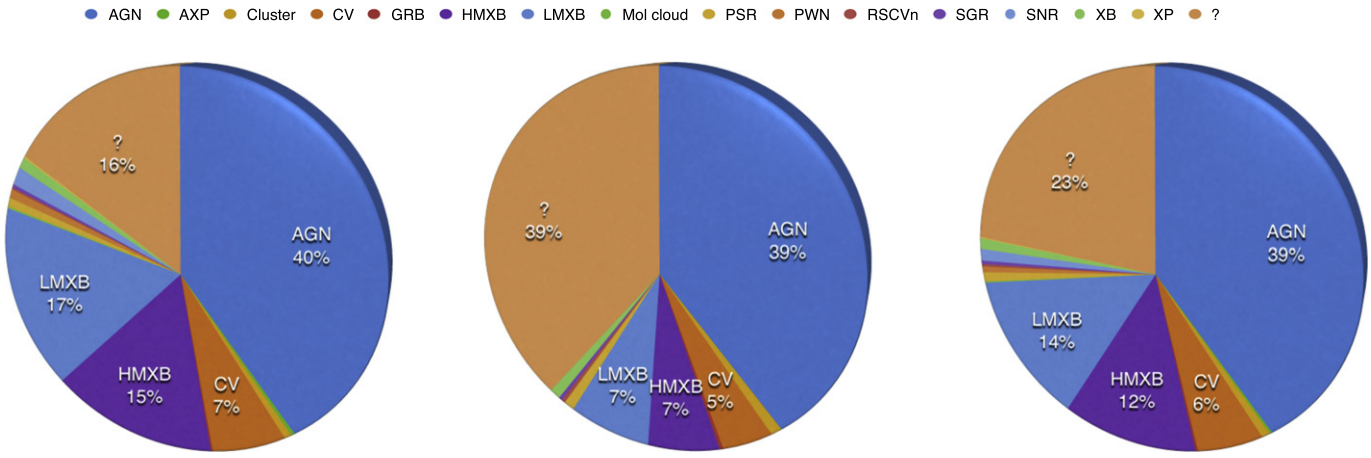

Figure 8. Source type distributions for (left) confirmed cat4 sources; (center) new cat1000 sources added since cat4; and (right) cat1000 overall.

4. DETAILED COMPARISON WITH 4th IBIS/ISGRI CATALOG

Of the 723 sources detected in the fourth IBIS/ISGRI catalog, 632 are listed in this new catalog, while 4 are not included because of the new methods employed to analyze the Galactic Center, and 87 are not included because they did not pass the new acceptance thresholds.

The sources that were given in cat4, but that were not detected by the cat1000 analysis, have been subjected to further inspection. While we would always expect some false positives in any catalog, the number of missing cat4 sources is far in excess of the expected level quoted in cat4. In total, 87 cat4 sources are not confirmed in cat1000, and breaking this subset of sources down by detection type, there is a clear trend toward these (assumed) false positives coming from the shorter outburst detections (Figure 7, left).

Further analysis of the 87 rejected sources shows that only 25 sources come from the stacked whole data set maps, which are optimized for persistent source detection. Even then, many of these persistent sources derive from low exposure (less than 200 ks) areas of the maps and so may be thought of as short exposure detections. Another 14 rejected sources derive from burst maps, which may be of any exposure but tend toward shorter timescales, 31 from revolution (so $\leqslant$200 ks exposure) maps, and 17 from short sequences of revolutions. The other very clear (and expected trend) is toward low-significance detections; only 12 of the missing cat4 sources were originally attributed a significance greater than 6σ. These trends are illustrated in Figure 7 (right), which shows the fraction of sources rejected between cat4 and cat1000 as a function of both duration and significance. We would expect a rejection rate of $\sim$1% based on the expected noise content of the persistent maps, but the rejection rates for sources that were detected on short timescales ($<$70 days) and at relatively low significance ($<6\sigma$) were much higher than that; in the worst case for the short outbursts below 5σ, only 1 in 2 sources have been confirmed by the new analysis. Outside of the region bounded by a duration of $<$70 days and a significance of $<6\sigma$ the rejection fraction falls to the expected levels. These results are consistent with, and may be explained in the context of, the simulations described in Section 2.4.

For the sources that are identified in shorter periods (bursts, revolutions, sequences) we have cross-checked the outbursts detected in cat1000 against those found in cat4. In many cases there is no time correlation, and we must conclude that these cat4 excesses were probably random bright periods in the light curve of a random point of sky, and should be considered false detections. We note here that the methods employed in cat1000 are much more robust, as all five main energy bands are searched for outbursts, and we expect time correlation between the bursts in at least two of the bands. Furthermore, we have operated with a much higher significance threshold for short outburst detection. However, the improved methods used in this work still only partially protect against the other likely explanation of false short bursts in cat4. Specifically, a short sequence of science windows where the data is hard to analyze due to noise, blended sources, or an incomplete catalog may give rise to strong image artefacts, and we have to assume the same conditions may persist from cat4 to cat1000. Therefore the detection of a burst at the same time in cat4 and cat1000, although strongly indicative, on its own is not considered 100% confirmation of source detection.

We must assume that those few rejected sources that were originally detected in persistent maps (i.e., by compiling all observations) and with long exposures were spurious detections of artefacts induced by the previous imaging software version, and are now better suppressed in OSA 9.0. Numerous changes were implemented in the software, instrument response models, and reference catalogs between OSA 7.0 and OSA 9.0. The use of a newer, improved base "cleaning" catalog will certainly have played a part in reducing the image noise levels. Long-term source variability should not cause a previously known source to be rejected. Since these previously detected sources are automatically included in our analysis, they should be detected despite a declining flux—we are confident that the bursticity analysis successfully identifies them as active during the earlier mission phases.

Following removal of those sources not confirmed in this work, we can re-analyze the source type distribution for the confirmed cat4 sources. The modified source type distribution (Figure 8(left) and Table 1) shows the success of the various follow-up campaigns, in that only 16% of the confirmed cat4 sources now lack an association with a specific type of object. Conversely, follow-ups on the 87 missing cat4 sources have largely failed to identify clear counterparts, with only 3 likely and 10 possible AGN associations being reported. Some random correlation with sources is to be expected, and in the extragalactic sky this is most likely to produce correlations with

Table 1
Source Type Numbers for Confirmed cat4 Sources, New cat1000 Sources Added since cat4 and cat1000 Overall

Type	cat4		cat1000 New		cat1000 Overall	
	Src	%	Src	%	Src	%
AGN	250	40%	119	39%	369	39%
?	100	16%	119	39%	219	23%
LMXB	106	17%	23	7.5%	129	14%
HMXB	96	15%	20	6.5%	116	12%
CV	42	7%	14	5%	56	6%
SNR	10	2%	0	<1%	10	1%
XB	6	<1%	3	1%	9	1%
PSR	5	<1%	3	1%	8	1%
Cluster	4	<1%	3	1%	7	1%
PWN	5	<1%	0	<1%	5	1%
SGR	2	<1%	1	<1%	3	<1%
AXP	2	<1%	0	<1%	2	<1%
GRB	1	<1%	1	<1%	2	<1%
RSCVn	1	<1%	1	<1%	2	<1%
Mol cloud	1	<1%	0	<1%	1	<1%
XP	1	<1%	0	<1%	1	<1%
Total	632		307		939	

the isotropic source populations (mostly AGNs and cataclysmic variables; CVs). Nevertheless, this low rate of association with known objects gives us further confidence that we have successfully identified a subset of likely false positive excesses.

5. RESULTS

This new catalog lists 939 sources detected with a systematic analysis of all public observations collected up to the end of 2010 and consisting of 8 years of *INTEGRAL* data (Table 2). Of these sources, 881 have a significance above the 5σ level and can be considered more secure detections, while the rest have a lower significance in the range of 4.5σ–5σ.

307 sources in this catalog are new entries with respect to cat4 (these are shown in bold font in the source list); some of them have been previously declared as *INTEGRAL* detections, or have already been included in the *INTEGRAL* reference catalog (Ebisawa et al. 2003). In particular, 60 sources have previously been discovered and reported in the literature with IGR designations. Furthermore, 127 sources are already listed either in other hard X-ray catalogs, mainly that of *Swift*/BAT, or previously reported elsewhere. Therefore the remaining 120 sources are reported as soft gamma-ray emitters for the first time in this work.

Table 1 shows the source distribution by class in this new catalog—as in previous catalogs the same main source classes are detected (HMXB, LMXB, CV, and AGN), including a large fraction of unassociated sources (23%). The same data are presented graphically in Figure 8 (center and right)

Compared to cat4 (Figure 8 (left)), there seems to be a slight change in the type fractions, i.e., overall the fraction of Galactic sources continues to reduce following the trend seen in previous catalogs. However, if we consider only the new entries (see Figure 8's center panel), it is evident that there is a large fraction of sources (39%) that still need to be identified and among them a significant number could eventually be of a Galactic nature.

This opens the path to a large program of follow-up work/observations, as has been successfully performed in the past. The follow-up program started 10 years ago with the release of the first IBIS catalog (Bird et al. 2004) and continued thereafter. Typically, the presence of a soft X-ray source in the IBIS error box has been used to reduce the soft gamma-ray positional uncertainty and hence enable optical and NIR follow-up observations. This process has been performed either by cross-checking with a number of available X-ray catalogs (e.g., with *ROSAT*; see Stephen et al. 2005; Stephen 2006), using IBIS itself (50%), or using additional observations with other missions such as *Swift* (27%), *Chandra* (17%), or *XMM*(5%).

As recently reviewed by Masetti et al. (2013), teams have so far pinpointed the nature of about 240 sources, which represents a large fraction of the unidentified objects listed in all previous IBIS surveys. The majority of these sources are AGNs (61%) followed by X-ray binaries (25%) and CVs (12%). Most of the AGNs are local Seyfert galaxies of type 1 and 2, while the largest fraction of Galactic binaries have a high-mass companion.

Overall this follow-up program has highlighted the key role played by *INTEGRAL* in discovering new classes of high-mass X-ray binaries (absorbed objects and supergiant fast X-ray transients), in detecting AGNs in the Zone of Avoidance, i.e., the area of the sky that is obscured by the Milky Way (Kraan-Kortoweg & Lahav 2000) and at high redshifts, as well as in confirming a population of magnetic CVs emitting above 20 keV. Follow-up work on unassociated sources in this new catalog has already started and hopefully will lead to further identifications.

6. COMPARISON WITH OTHER RECENT SOFT GAMMA-RAY CATALOGS

In this section we make a brief comparison between this catalog and two other soft gamma-ray surveys.

The first is that of Krivonos et al. (2012), which includes a very similar data set (up to revolution 1013) but only considers sources in the Galactic Plane. In addition Krivonos et al. (2012) used different software methods and slightly different energy bands within their data analysis to achieve a claimed identification completeness of 0.91. As well as allowing them to perform population studies on a good statistical basis (see Lutovinov et al. 2013), this level of completeness provides a good comparison for this work. Krivonos et al. (2012) identified 392 sources above a 5σ detection threshold, and this number increases to 402 if the detection threshold is lowered to 4.8σ. Comparison with our catalog indicates that only 15 of their sources are not present in our list, and of those, 12 have a detection significance below 5σ in at least 1 of the 3 energy bands used in the Krivonos catalog. The degree of agreement is thus ~99%, consistent with the statistical uncertainties associated with the two methods.

Second, we have also cross-correlated our source list with that of the 70-month *Swift*/BAT survey (Baumgartner et al. 2013). This catalog reports 1171 hard X-ray sources detected above a significance threshold of 4.8σ in the 14–195 keV energy band. So far this is the most sensitive and uniform survey in the soft gamma-ray band, reaching a limiting flux sensitivity of 1.34×10^{-11} erg s^{-1} cm^{-2} over 90% of the sky. Due to the satellite observing strategy, the

Table 2
IBIS Catalog of 1000 Orbits

Name[a]	R.A.	decl.	Error[b]	F20–40[c]	F40–100[c]	Type[d]	Vari[e]	Signif[f]	Exposure[g]
IGR J00040+7020	1.006	70.321	2.84	0.8 ± 0.1	1.0 ± 0.2	AGN, Sy2	···	9.2	3391
	Detected as a persistent source in the 20–100 keV band.								
IGR J00234+6141	5.74	61.685	2.66	0.7 ± 0.1	0.3 ± 0.1	CV, IP	···	9.9	4777
	Detected as a persistent source in the 17–30 keV band.								
GRB041219A IGR J00245+6251	6.117	62.843	1.44	<0.1	0.3 ± 0.1	GRB	YY	20.1	4812
	Detected in a 0.6 day outburst from MJD = 53358.0.								
4U 0022+63	6.321	64.159	2.21	0.7 ± 0.1	0.8 ± 0.1	SNR	···	12.2	4718
	Detected as a persistent source in the 18–60 keV band.								
IGR J00256+6821	6.374	68.357	2.44	0.7 ± 0.1	1.1 ± 0.1	AGN, Sy2	···	10.9	4072
	Detected as a persistent source in the 20–100 keV band.								
V709 Cas RX J0028.8+5917	7.204	59.289	0.61	4.4 ± 0.1	2.7 ± 0.1	CV, IP	···	60.1	4517
	Detected as a persistent source in the 18–60 keV band.								
IGR J00291+5934	7.263	59.572	0.41	2.0 ± 0.1	2.4 ± 0.1	LMXB, XP, T	Y	109.7	4537
	Detected in a 12.3 day outburst from MJD = 53337.5.								
IGR J00333+6122	8.326	61.462	2.55	0.7 ± 0.1	0.9 ± 0.1	AGN, Sy1.5	···	10.4	4697
	Detected as a persistent source in the 20–100 keV band.								
SWIFT J0034.5-7904 1RXS J003422.2-790525	8.579	−79.11	5.14	0.7 ± 0.2	<0.6	AGN, Sy1	···	4.8	1153
	Detected as a persistent source in the 17–30 keV band.								
1ES 0033+595	8.969	59.835	1.50	1.4 ± 0.1	0.9 ± 0.1	AGN, BL Lac	···	19.1	4520
	Detected as a persistent source in the 17–30 keV band.								

Notes.
[a] Names in boldface indicate new detections since the fourth IBIS/ISGRI catalog.
[b] Position errors expressed as radius of 90% confidence circle in arcminutes.
[c] Time-averaged flux expressed in units of mCrab; appropriate conversion factors are: (20–40 keV) 10 mCrab = 7.57×10^{-11} erg cm^{-2} s^{-1} = 1.71×10^{-3} ph cm^{-2} s^{-1}; (40–100 keV) 10 mCrab = 9.42×10^{-11} erg cm^{-2} s^{-1} = 9.67×10^{-4} ph cm^{-1} s^{-1}.
[d] Source type classifications: A—atoll source (neutron star), AGN—active galactic nuclei, AXP—anomalous X-ray pulsar, B—burster (neutron star), Be—B-type emission-line star, BH—black hole (confirmed mass evaluation), BHC—black hole candidate, BL—broad line, cluster—cluster of galaxies, CV—cataclysmic variable, D—dipping source, DN—dwarf nova, G—globular cluster X-ray source, GRB—gamma-ray burst, HMXB—high-mass X-ray binary, IP—intermediate polar, LMXB—low-mass X-ray binary, M—microquasar, Mol Cloud—molecular cloud, NL—narrow line, NS—neutron star, P—polar, PSR—radio pulsar, PWN—pulsar wind nebula, QSO—quasar, RG—radio galaxy, SFXT—supergiant fast X-ray transient, SG—supergiant, SGR—soft gamma-ray repeater, SNR—supernova remnant, Sy—Seyfert galaxy, Symb—symbiotic star, T—transient source, XB—Galactic X-ray binary, XBONG—X-ray bright, optically normal galaxy, XP—X-ray pulsar, Z = Z-type source (neutron star).
[e] Variability indicator; see Section 3 for details.
[f] Maximum significance in a single map; see notes on individual sources for detection method.
[g] Corrected on-source exposure (ks).

(This table is available in its entirety in machine-readable form.)

Swift/BAT all-sky survey is very uniform, which explains why most of the reported sources (about 60%) are of extragalactic nature. Comparing the catalog of this work with that of Baumgartner et al. (2013) results in 565 correlations within a distance of 400″. Of these, 311 are of extragalactic nature, 246 are Galactic sources, and the rest lack a precise association. Figure 9 shows the number of sources detected by BAT and IBIS as a function of Galactic longitude, either within 10° of the Galactic Plane (upper panel), or more than 10° from the Plane (lower panel). The differences between these two surveys is immediately apparent. It is clear that *INTEGRAL* has been more effective at finding soft gamma-ray emitting sources along the Galactic Plane, and particularly along the directions of the spiral arms. *Swift*/BAT, as a result of its larger FOV and more uniform all-sky exposure, is more effective on the extragalactic sky. Thus Figure 9 emphasizes the great complementarity between these two missions, and the source catalogs they produce.

6.1. Concluding Comments

As predicted in the fourth IBIS catalog, with the further data available from AO6 and AO7, this latest catalog shows a large increase in the populations in the sky beyond the Galactic Plane —seen in both the AGN class (more than 100 new sources) and CVs. As with all previous catalogs exploiting new data sets, there is a large fraction (23%) of unidentified sources that will require further study, and a robust follow-up program is essential for the weak persistent examples. Transient detections represent a greater challenge for follow-up due to the serendipitous nature of their discovery. A characterization of the transients based on their outburst duration, timing, and spectral properties, and quiescent emission will be needed to further identify their nature(s).

Once again, the soft gamma-ray sky has shown itself to be both well-populated and highly variable, as the advent of missions with survey capabilities like *INTEGRAL* and *Swift* has demonstrated over the last 10 years, and continues to

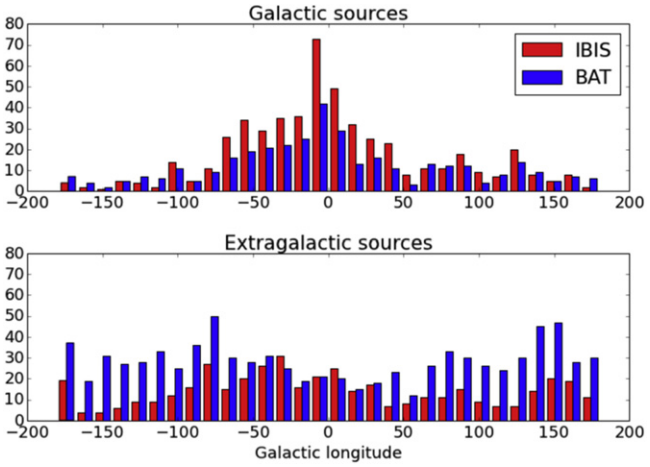

Figure 9. (Upper panel) Distribution of sources detected by *INTEGRAL*/IBIS (red) and *Swift*/BAT (blue) as a function of Galactic longitude. (Upper panel) sky region within 10° of the Galactic Plane; (lower panel) sky more than 10° from the Plane.

demonstrate. Both *INTEGRAL* and *Swift* continue their highly complementary monitoring programs, and continue to discover new sources. Studies using long term light curves and spectral evolution are now possible and can be performed well beyond 100 keV. With the information reported in the current work and in combination with the recent results from the 11-year survey above 100 keV (Krivonos et al. 2015), one can already derive a hardness ratio in the energy bands 20–100/100–150 keV and may understand the general properties of the 108 common sources. We believe this will prove an invaluable data set for studying the high-energy behavior of different classes of sources. By comparing these catalog data with observations performed at lower (X-ray band) and higher (MeV and GeV bands) energies, it will be possible to create broadband spectra and therefore a unique and comprehensive view of many of the objects in our sky.

We acknowledge the funding from Italian Space agency financial and programmatic support via ASI/INAF agreement No. 2013-025-R.0. A.B.H. acknowledges support from a Marie Curie International Outgoing Fellowship within the 7th European Community Framework Program (FP7/20072013) under grant agreement No. 275861.

This research has made use of: data obtained from the High Energy Astrophysics Science Archive Research Center (HEASARC) provided by the NASA Goddard Space Flight Center; the SIMBAD database operated at CDS, Strasbourg, France; and the NASA /IPAC Extragalactic Database (NED) operated by the Jet Propulsion Laboratory, California Institute of Technology, under contract with NASA.

REFERENCES

Bassani, L., Molina, M., Malizia, A., et al. 2006, ApJ, 636, 65
Baumgartner, T. J., Markwardt, S. G. K., Barthelmy, S., et al. 2013, ApJS, 207, 19
Beckmann, V., Soldi, S., Ricci, C., et al. 2009, A&A, 505, 417
Bertin, E., & Arnouts, S. 1996, A&AS, 117, 393
Bird, A. J., Barlow, E. J., Bassani, L., et al. 2004, ApJ, 607, 33
Bird, A. J., Barlow, E. J., Bassani, L., et al. 2006, A&A, 445, 869
Bird, A. J., Bazzano, A., Bassani, L., et al. 2010, ApJS, 186, 1
Bird, A. J., Malizia, A., Bazzano, A., et al. 2007, ApJS, 170, 175
Bottacini, L., Ajello, M., & Griener, J. 2012, ApJS, 201, 34
Bouchet, L., Jourdain, E., Roques, J.-P., et al. 2008, ApJ, 679, 1315
Ebisawa, K., Bourban, G., Bodaghee, A., Mowlavi, N., & Courvoisier, T. J.-L 2003, A&A, 411, 59
Gros, A., Goldwurm, A., Cadolle-Bel, M., et al. 2003, A&A, 411, L179
Kraan-Kortoweg, R. C., & Lahav, O. 2000, A&ARv, 10, 211
Krivonos, R., Tsygankov, S., Revnivtsev, M., et al. 2010, A&A, 523, A61
Krivonos, R., Tsygankov, S., Lutovinov, A., et al. 2012, A&A, 545, A27
Krivonos, R., Tsygankov, S., Lutovinov, A., et al. 2015, MNRAS, 448, 3766
Lebrun, F., Leray, J. P., Lavocat, P., et al. 2003, A&A, 411, L141
Liu, Q. Z., van Paradijs, J., & van den Heuvel, E. P. J. 2007, A&A, 469, 807
Lutovinov, A., Revnivtsev, M., Gilfanov, M., & Sunyaev, R. 2007, in ESA Special Publication 622, Proc. of the 6th Integral Workshop, ed. S. Grebenev, R. Sunyaev, & C. Winkler (Noordwijk: ESA), 241
Lutovinov, A., Revnivtsev, M., Tsygankov, S., & Krivonos, R. 2013, MNRAS, 431, 327
Malizia, A., Bassani, L., Bazzano, A., et al. 2012, MNRAS, 426, 1750
Masetti, N., Parisi, P., Palazzi, E., et al. 2013, A&A, 556, 120
Revnivtsev, M., Lutovinov, A., Churazov, E., et al. 2008a, A&A, 491, 209
Revnivtsev, M., Sazonov, S., Krivonos, R., et al. 2008b, A&A, 489, 1121
Sazonov, S., Revnivtsev, M., Krivonos, R., et al. 2007, A&A, 462, 57
Scaringi, S., Bird, A. J., Norton, A. J., et al. 2010a, MNRAS, 401, 2207
Scaringi, S., Bird, A. J., Hill, A. B., et al. 2010b, A&A, 516, 75
Stephen, J. B. 2006, A&A, 445, 869
Stephen, J. B., Bassani, L., Molina, M., et al. 2005, A&A, 432, 49
Ubertini, P., Lebrun, F., Di Cocco, G., et al. 2003, A&A, 411, L131